Environmental Science & Technology

Article

pubs.acs.org/est

Oxidation of Benzene by Persulfate in the Presence of Fe(III)- and Mn(IV)-Containing Oxides: Stoichiometric Efficiency and Transformation Products

Haizhou Liu,[†] Thomas A. Bruton,[‡] Wei Li,[†] Jean Van Buren,[‡] Carsten Prasse,[‡] Fiona M. Doyle,[§] and David L. Sedlak*,[‡]

[†]Department of Chemical and Environmental Engineering , University of California at Riverside, Riverside, California 92521 United States

[‡]Department of Civil and Environmental Engineering and [§]Department of Material Science and Engineering, University of California at Berkeley, Berkeley, California 94720 United States

Supporting Information

ABSTRACT: Sulfate radical ($SO_4^{\bullet-}$) is a strong, short-lived oxidant that is produced when persulfate ($S_2O_8^{2-}$) reacts with transition metal oxides during in situ chemical oxidation (ISCO) of contaminated groundwater. Although engineers are aware of the ability of transition metal oxides to activate persulfate, the operation of ISCO remediation systems is hampered by an inadequate understanding of the factors that control $SO_4^{\bullet-}$ production and the overall efficiency of the process. To address these shortcomings, we assessed the stoichiometric efficiency and products of transition metal-catalyzed persulfate oxidation of benzene with pure iron- and manganese-containing minerals, clays, and aquifer solids. For most metal-containing solids, the stoichiometric efficiency, as determined by the loss of benzene relative to the loss of persulfate, approached the theoretical maximum. Rates of production of $SO_4^{\bullet-}$ or hydroxyl radical ($HO^{\bullet}$) generated from radical chain reactions were affected by the concentration of benzene, with rates of $S_2O_8^{2-}$ decomposition increasing as the benzene concentration increased. Under conditions selected to minimize the loss of initial transformation products through reaction with radicals, the production of phenol only accounted for 30%−60% of the benzene lost in the presence of O_2. The remaining products included a ring-cleavage product that appeared to contain an α,β-unsaturated aldehyde functional group. In the absence of O_2, the concentration of the ring-cleavage product increased relative to phenol. The formation of the ring-cleavage product warrants further studies of its toxicity and persistence in the subsurface.

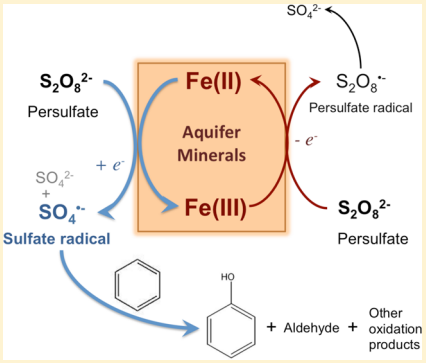

INTRODUCTION

In situ chemical oxidation (ISCO) has been used for several decades for the remediation of contaminated groundwater and aquifer solids.[1] Recently, persulfate ($S_2O_8^{2-}$) has become popular as an oxidant in ISCO systems due to its ability to oxidize a variety of contaminants.[2,3] When persulfate is injected into the subsurface without any other additives, it is activated by Fe(III)- and Mn(IV)-containing oxides to produce sulfate radical ($SO_4^{\bullet-}$),[4,5] an oxidant that reacts with a variety of contaminants.[6−16] $SO_4^{\bullet-}$ also can be converted to hydroxyl radical ($HO^{\bullet}$) under alkaline conditions,[17−19] or in the presence of chloride.[10,20,21] The effectiveness of ISCO depends on the rate of $S_2O_8^{2-}$ activation and the yield of $SO_4^{\bullet-}$ and other reactive radicals. $S_2O_8^{2-}$ activation rates and oxidant yields appear to be affected by the nature of the minerals and aquifer solids, the groundwater composition, and the presence of organic contaminants that can initiate radical chain reactions that convert $S_2O_8^{2-}$ into $SO_4^{\bullet-}$ and other reactive radicals.[2,3,5,22]

To characterize the mechanism through which oxidants are activated in ISCO systems, it is important to understand the stoichiometric efficiency of the reaction (i.e., the number of moles of benzene transformed per mole of oxidant activated). For example, measurement of the yield of $HO^{\bullet}$ in Fenton-like reactions catalyzed by metal oxides and aquifer solids indicated that less than 2% of the H_2O_2 was converted into $HO^{\bullet}$ and that aquifer solids with the highest ratios of Fe(III) oxides to Mn(IV) oxides exhibited the highest $HO^{\bullet}$ yield.[23,24] This type of information can be useful in the selection and the deployment of ISCO oxidants and the development of approaches to increase oxidant yields for ex situ treatment systems.

Quantification of the stoichiometric efficiency in $S_2O_8^{2-}$-based ISCO systems is complicated by the slow rate of $S_2O_8^{2-}$ loss and the complex radical chain reactions that occur in groundwater. To provide insight into the factors controlling persulfate activation and the mechanisms through which

Received: October 1, 2015
Revised: December 17, 2015
Accepted: December 20, 2015
Published: December 21, 2015

DOI: 10.1021/acs.est.5b04815
Environ. Sci. Technol. 2016, 50, 890−898

organic contaminants are transformed, we conducted experiments in which persulfate was activated by Fe(III) oxides, Mn(IV) oxides, clays, and aquifer solids under conditions comparable to those in the groundwater, with benzene serving as a representative organic contaminant. By measuring the rates at which benzene and persulfate disappeared, as well as the rate of formation of oxidation products, it was possible to gain insight into the mechanism of persulfate activation by metal-containing solids and the complex nature of reactions initiated by $SO_4^{\bullet-}$ when organic contaminants are present.

MATERIALS AND METHODS

A detailed description of the experimental setup and materials was presented previously.[5] A brief summary is included below with specific details included as Text S1. A total of four types of pure minerals were studied: amorphous ferrihydrite ($Fe(OH)_{3(s)}$), goethite (α-$FeOOH_{(s)}$), pyrolusite (β-$MnO_{2(s)}$), and silica ($SiO_{2(s)}$). Two clay materials (nontronite and montmorillonite) and five aquifer solids collected from relatively uncontaminated locations at sites undergoing remediation were also studied. Details on the minerals, clays, and aquifer solids and their characteristics are provided in Table S1 and Text S1. For $SO_4^{\bullet-}$ generation experiments, a 1 mM benzene solution was freshly prepared from anhydrous benzene (purity ≥99.8%, Sigma-Aldrich Inc.) in a 1-L glass volumetric flask filled with deionized (DI) water without headspace. The dissolved O_2 concentration in all solutions was adjusted by purging with air, N_2, or pure O_2. Details on the control of dissolved O_2 are provided as Text S2. The 1 L solution was buffered at pH 8.0 with 50 mM borate. In some experiments, synthetic groundwater was used to assess benzene oxidation by persulfate activation. The chemical composition of the synthetic groundwater was reported previously and reported as Table S2.[5]

To start an experiment, we quickly mixed 250 mL of the benzene solution with a predetermined amount of solids in a 300-mL beaker, and persulfate was added to yield an initial concentration of 1 mM using aliquots of a freshly prepared 100 mM $K_2S_2O_8$. After mixing, the suspension was immediately transferred to multiple sealed glass tubes with no headspace and placed on a rotating mixer (Labquake Tube Rotators, Thermo Scientific Inc.). At predetermined sampling intervals, each sealed sacrificial tube reactor was centrifuged, and a sample was taken.

Persulfate was measured using the KI colorimetric method[25] with a λ-14 UV spectrophotometer (PerkinElmer Inc., Waltham, MA). Benzene and its oxidation products were analyzed on a Waters Alliance 2695 HPLC (Waters Corp., Milford, MA) equipped with a diode array detector and a Waters Symmetry-C18 column. Dissolved O_2 concentrations were measured as the reaction proceeded using a YSI Model 58 oxygen probe (YSI Inc., Yellow Springs, OH).

The unknown oxidation product was characterized by high-resolution mass spectrometry (HRMS), which was conducted using an Agilent 6520 quadrupole time-of-flight (Q-TOF) instrument coupled to an Agilent 1200 HPLC. Details of the chromatography and its operating conditions were included as Text S3. The chemical structure of the unknown product was further characterized by nuclear magnetic resonance (NMR). To prepare the sample, we used solid-phase extraction (SPE) to separate the unknown compound from benzene and phenol and to concentrate the sample. Details of the SPE procedure were included as Text S4. This procedure was repeated several times to achieve an overall enrichment factor of 200. The final sample was subjected once more to the SPE procedure using D_2O (pH 2) for washing of the cartridge and CH_3CN-d_3 for elution of the unknown. NMR analysis (^{1}H NMR, ^{1}H,^{1}H–COSY, ^{1}H,^{1}H-NOESY, ^{1}H, and ^{13}C-HSQC) was performed within 1 day to minimize degradation of the unknown compound. NMR spectra were acquired on a Bruker Avance 600 MHz instrument. To assess the formation of aldehyde oxidation products, we carried out experiments by mixing 10 mM bisulfite with the SPE-enriched unknown product. The formation of an aldehyde-bisulfite adduct was monitored by LC/MS using an Agilent 1200 series HPLC coupled with an Agilent 6410 Triple Quad LC/MS over 2 h.

RESULTS AND DISCUSSION

Persulfate activation. Persulfate concentrations decreased slowly over the course of the experiments (Figure 1). In thermal controls without minerals, the persulfate concentration decreased by less than 3% over 32 days, which was consistent with previously published data on thermal activation.[5,26] Persulfate loss in the presence of goethite was slow, with approximately 5% of persulfate lost after 32 days. However, when 50 g/L of goethite and 1 mM of benzene were both present, 15% of the persulfate disappeared during the experiment. Similarly, 25% of the persulfate disappeared in the presence of pyrolusite and benzene after 32 days (Figure 1). The presence of silica had a negligible effect on persulfate loss rate when benzene was present compared to the thermal control.

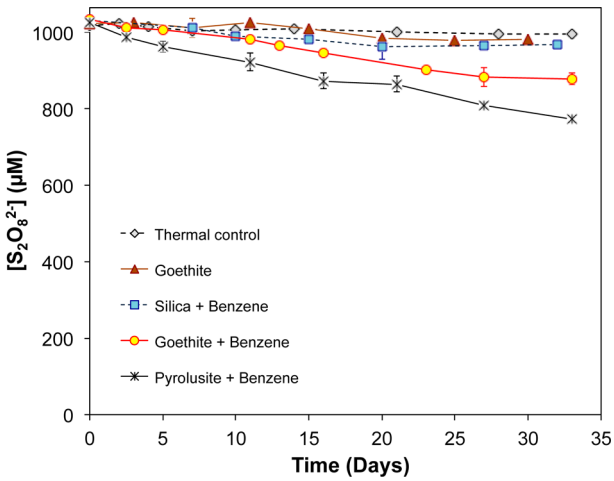

Figure 1. Changes of persulfate concentrations during mineral-catalyzed activation. Minerals were present at 50 g/L, and pH was buffered at 8.0 with 50 mM borate. When present, benzene was 1000 μM.

The decrease of persulfate concentration was accompanied by a loss of benzene (Figure 2). In thermal controls containing only benzene, the benzene concentration was constant over the 32-day experiment, indicating no volatilization of benzene from the sealed reactors. In goethite controls containing only goethite and benzene but no persulfate, complete recovery of adsorbed benzene from the goethite was achieved. Particle-associated benzene (i.e., the adsorbed fraction recovered by acetonitrile extraction) accounted for approximately 10–20% of the added benzene in the goethite control and 5–10% in adsorption control experiments with other solids. Full recovery

DOI: 10.1021/acs.est.5b04815
Environ. Sci. Technol. 2016, 50, 890–898

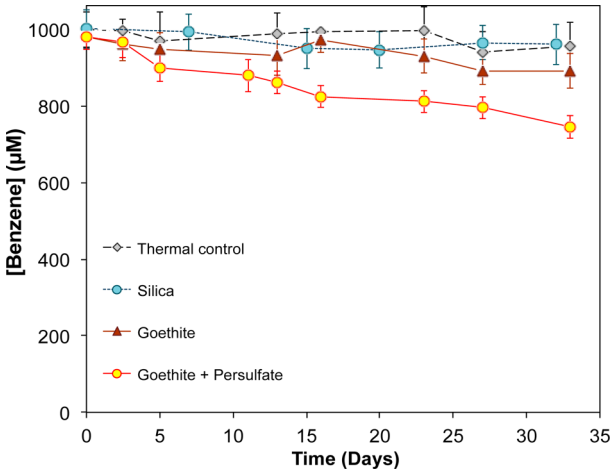

Figure 2. Changes of total benzene concentration during persulfate activation in the presence of 50 g/L of goethite. pH was buffered at 8.0 with 50 mM borate. Benzene concentration includes aqueous and adsorbed benzene recovered by extraction. Initial persulfate was 1000 μM.

of adsorbed benzene by acetonitrile extraction was also achieved with ferrihydrite, pyrolusite, and the aquifer solids (Figure S1). When 1 mM of persulfate was added in the presence of 50 g/L goethite, the benzene concentration decreased from 1000 μM to approximately 750 μM during the 32 day experiment (Figure 2). Similar results were observed for all other Fe(III)- and Mn(IV)-containing minerals and all aquifer solids except silica (Figures S2–S10).

The acceleration of the rate of persulfate loss in the presence of benzene was most likely caused by a series of chain reactions that produced intermediate organic radicals. Experiments conducted in the absence of benzene were consistent with a mechanism in which persulfate was activated by Fe(III)- and Mn(IV)-containing minerals (denoted as $\equiv M^{n+}$) to generate $SO_4^{\bullet-}$ and $S_2O_8^{\bullet-}$:[2,5]

$$\equiv M^{n+} + S_2O_8^{2-} \rightarrow \equiv M^{(n-1)+} + S_2O_8^{\bullet-} \quad \text{(R1)}$$

$$\equiv M^{(n-1)+} + S_2O_8^{2-} \rightarrow \equiv M^{n+} + SO_4^{\bullet-} + SO_4^{2-} \quad \text{(R2)}$$

$S_2O_8^{\bullet-}$, the product of the reaction between Fe(III) and $S_2O_8^{2-}$, can be involved in radical chain reactions that lead to the generation of additional $SO_4^{\bullet-}$ or other radicals,[7,29] as summarized in Text S5. Other mechanisms of persulfate activation by Fe(III)- and Mn(IV)-containing minerals also are possible. Additional research is needed to elucidate the mechanism of this process.

In the absence of benzene, $SO_4^{\bullet-}$ can react with persulfate to generate additional $S_2O_8^{\bullet-}$ radicals:[27,28]

$$SO_4^{\bullet-} + S_2O_8^{2-} \rightarrow S_2O_8^{\bullet-} + SO_4^{2-} \qquad k_3 = 6.3 \times 10^5\ M^{-1}s^{-1} \quad \text{(R3)}$$

$SO_4^{\bullet-}$ can also react with water or OH^- to generate $HO^\bullet$:[29−31]

$$SO_4^{\bullet-} + H_2O \rightarrow SO_4^{2-} + HO^\bullet + H^+ \qquad k_4 = 660\ s^{-1} \quad \text{(R4)}$$

$$SO_4^{\bullet-} + OH^- \rightarrow SO_4^{2-} + HO^\bullet \qquad k_5 = 7 \times 10^7\ M^{-1}s^{-1} \quad \text{(R5)}$$

Under the condition studied here (i.e., $[S_2O_8^{2-}]$ = 1 mM; pH = 8]), reactions R3 and R4 each accounted for approximately half of the $SO_4^{\bullet-}$ loss, and reaction R5 was unimportant.

In addition, three reactions can act as sinks for $HO^\bullet$:[16,28,32]

$$HO^\bullet + HO^\bullet \rightarrow H_2O_2 \qquad k_6 = 5.5 \times 10^9\ M^{-1}s^{-1} \quad \text{(R6)}$$

$$HO^\bullet + SO_4^{\bullet-} \rightarrow HSO_5^- \qquad k_7 = 1.0 \times 10^{10}\ M^{-1}s^{-1} \quad \text{(R7)}$$

$$HO^\bullet + S_2O_8^{2-} \rightarrow S_2O_8^{\bullet-} + OH^- \qquad k_8 = 1.4 \times 10^7\ M^{-1}s^{-1} \quad \text{(R8)}$$

Considering the low steady-state concentrations of $HO^\bullet$ and $SO_4^{\bullet-}$ relative to $S_2O_8^{2-}$, reaction R8 was the main sink for $HO^\bullet$. Under these conditions, the steady-state concentration of $SO_4^{\bullet-}$ should have been approximately 20 times higher than that of $HO^\bullet$ (see Text S6 for details).

The overall pathways of radical generation in the absence of benzene are illustrated in Scheme 1. Experimental data indicate

Scheme 1. Illustration of Major Radical Chain Reactions When Persulfate Is Activated by Transition Metal Oxide in the Absence of Benzene or Other Contaminants[a]

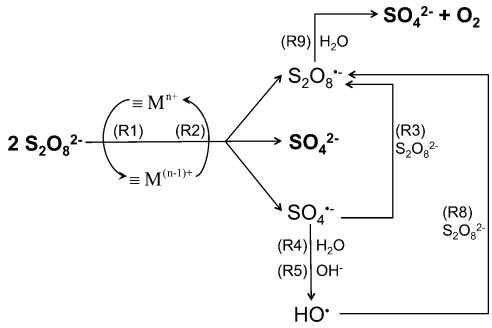

[a]Sulfate and oxygen are the final products of persulfate activation.

that SO_4^{2-} and O_2 were always the final products of $S_2O_8^{2-}$ activation.[5] In the absence of benzene, metal-catalyzed activation of $S_2O_8^{2-}$ resulted in oxidation of water and production of sulfuric acid:[30,33]

$$S_2O_8^{\bullet-} + \frac{3}{2}H_2O \rightarrow 2SO_4^{2-} + \frac{3}{4}O_2 + 3H^+ \quad \text{(R9)}$$

The overall reaction can be described as follows:

$$S_2O_8^{2-} + H_2O \rightarrow \frac{1}{2}O_2 + 2SO_4^{2-} + 2H^+ \quad \text{(R10)}$$

Benzene Oxidation Mechanism and Product Distribution. Although it is difficult to ascertain the mechanism through which benzene is oxidized in this complex system, it is possible to propose pathways that account for the observed products by considering previous studies involving benzene, $SO_4^{\bullet-}$ and other reactive species (Scheme 2). Other reaction pathways also could account for these products and should be considered in future research. When it reacts with benzene, $SO_4^{\bullet-}$ abstracts an electron from benzene to produce a short-lived cation radical ($C_6H_6^{\bullet+}$)[7,13,34,35] (reaction 11 in Scheme 2; $k_{10} = 3 \times 10^9\ M^{-1}\ s^{-1}$). Under conditions employed in this study (i.e., initial [benzene] = 1 mM and [persulfate] = 1 mM), k_{11}[benzene] $\gg k_3[S_2O_8^{2-}]$), the majority of the $SO_4^{\bullet-}$ produced during $S_2O_8^{2-}$ activation is consumed by benzene.

DOI: 10.1021/acs.est.5b04815
Environ. Sci. Technol. 2016, 50, 890−898

Scheme 2. Proposed Radical Chain Reactions Involving $S_2O_8^{2-}$ Activation, $SO_4^{\bullet-}$ Generation, Chain Propagation with Benzene and Organic Peroxy Radical, and Formation of Phenol and the Aldehyde Product[a]

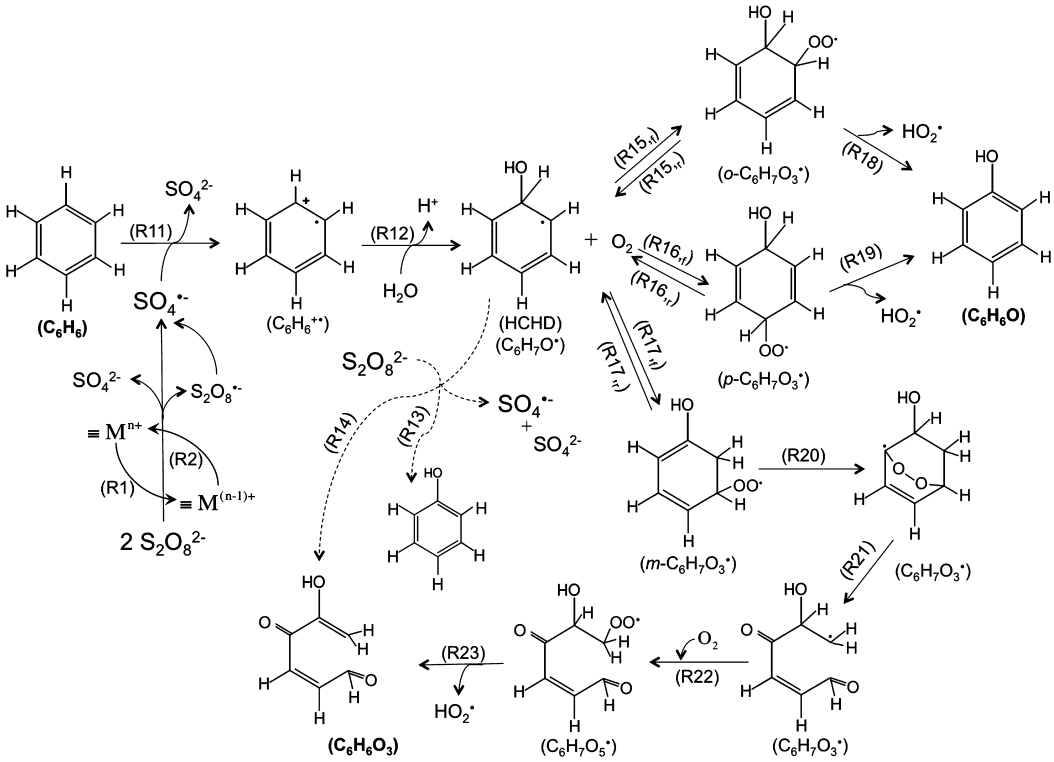

[a]The aldehyde shown is one possible product that is consistent with the NMR analysis. Dashed lines indicate pathways in oxygen-free conditions. The phenol and aldehyde are not the terminal oxidation products and can be further oxidized.

Table 1. Production of Phenol as a Primary Oxidation Product from Benzene Oxidation by Persulfate Activation and the Impact of Dissolved O_2

solids		product distribution (−(Δ[phenol]/Δ[benzene]) × 100%)		
		$[O_2]$ = 3 μM	$[O_2]$ = 250 μM	$[O_2]$ = 410 μM
	silica	24% ± 2%	45% ± 4%	–
minerals	goethite	18% ± 8%	30% ± 11%	62% ± 11%
	ferrihydrite	32% ± 13%	57% ± 16%	–
	pyrolousite	27% ± 11%	34% ± 9%	–
clays	nontronite	–	38% ± 13%	–
	montmorillonite	–	28% ± 2%	–
aquifer solids	AWBPH	–	73% ± 7%	–
	AFTCS	–	100% ± 5%	–
	CAROL	–	73% ± 4%	–
	CADOU	–	15% ± 6%	–
	AMTAL	–	25% ± 2%	–

$C_6H_6^{\bullet+}$ can react with H_2O to form an intermediate, known as hydroxylcyclohexadienyl (HCHD) radical (i.e., $C_6H_7O^{\bullet}$, reaction 12 in Scheme 2).[34] HCHD radical was also observed during the oxidation of benzene by $HO^{\bullet}$ via the OH addition.[15,36] Further consumption of $S_2O_8^{2-}$ by its reaction with HCHD and other radical species may have been partially responsible for the faster loss of persulfate when benzene was present (Figure 1), as illustrated by reactions 13 and 14 in Scheme 2. These reactions act as chain propagation reactions that accelerate the consumption of persulfate in the presence of benzene (Figure 1A).

HCHD radical can react with O_2 either in the *ortho*, *para*, or *meta* position to produce three isomers of organic peroxy radicals, i.e., *o*-$C_6H_7O_3^{\bullet}$ and *m*-$C_6H_7O_3^{\bullet}$ (reactions 15−17 in Scheme 2),[36] which subsequently eliminate hydroperoxy radical ($HO_2^{\bullet}$) to produce phenol (reactions 18−19 in Scheme 2).[36,37] At circumneutral pH values, $HO_2^{\bullet}$ dissociates into $O_2^{\bullet-}$, which undergoes bimolecular dismutation or metal-catalyzed dismutation to produce H_2O_2.[5,38] Only a small fraction of H_2O_2 formed in this process (i.e., < 2%) produced $HO^{\bullet}$ through Fenton-like reactions at iron- and manganese-containing solid surfaces. Most of H_2O_2 is converted to H_2O and O_2 through nonradical pathways.[24,39,40] Therefore, H_2O_2 produced through dismutation had a negligible effect on benzene degradation or persulfate activation.

The mechanism described above indicates that phenol should be the primary product of benzene oxidation.[36,37,41] After phenol was produced, further reaction with oxidants

DOI: 10.1021/acs.est.5b04815
Environ. Sci. Technol. 2016, 50, 890−898

could result in the formation of poly hydroxylated compounds, followed by the eventual production of ring-cleavage products.[3,37−42] However, under conditions employed in these experiments (i.e., conversion of less than 35% of the benzene), a significant production of these later products was not expected. Oxygen addition at the *ortho*- and *para*-position (reaction 15) was the mechanism[36] through which phenol was formed (see Text S7).

Simultaneous quantification of benzene loss and phenol production indicated that phenol accounted for approximately 30% to 60% of the benzene loss under air-saturated conditions (Table 1). Loss of phenol due to reaction with $HO^{\bullet}$ or $SO_4^{\bullet-}$ after it was formed could not account for the discrepancy between benzene loss and phenol formation (Text S8). Inspection of the chromatogram of samples obtained after persulfate was activated by minerals in the presence of benzene indicated the presence of an unknown product in addition to phenol (Figure S11A). The UV spectrum of this product exhibited absorption maxima at 276 and 361 nm (Figure S11B), which is similar to the reported spectra of a six-carbon aldehyde compound (i.e., hydroxylmucondialdehyde) detected when benzene was oxidized by $HO^{\bullet}$ produced by continuous radiolysis in the presence of O_2.[36,41,43,44]

Analysis of the unknown ring-cleavage product by Q-TOF LC/MS revealed an exact mass of m/z 125.0246, corresponding to the sum formula $C_6H_5O_3$ (Figure S11−C). MS/MS experiments further revealed the cleavage of CO (fragments: m/z of 97.0296, $C_5H_5O_2$; m/z of 69.0250, C_4H_5O), indicating the presence of two −C═O moieties.[45] Increasing the collision energy yielded an additional fragment at m/z 79.0180 (C_5H_3O), suggesting cleavage of H_2O from fragment $C_5H_5O_2$. Q-TOF analysis suggests the presence of two −C═O functional groups with one having a hydroxyl group in the α-position.

^{1}H NMR results confirmed the presence of an aldehyde group as evidenced by the presence of a characteristic shift at 9.32 ppm (Figure S12). Results from the NOESY experiments further indicated coupling of the aldehyde proton to two protons with chemical shifts of 7.44 and 6.93 ppm, thus suggesting the presence of an α,β-unsaturated aldehyde moiety.[46] The identity of the remaining part of the molecule could not be further elucidated because the results were inconclusive. Although the signal at 8.63 ppm in the ^{1}H NMR spectrum might suggest the presence of an additional aldehyde moiety,[46] as indicated by high-resolution MS analysis, integration of the signals in the ^{1}H NMR spectrum revealed the presence of two protons for chemical shift 8.63 ppm, thus excluding an aldehyde moiety. Rather, the results suggested a terminal sp^2 carbon was adjacent to an electron withdrawing environment, possibly a hydroxylated carbon bonded to a carbonyl, which might explain the atypically far downfield shift of 8.63 ppm and the weak coupling with the enal fragment of the molecule seen in the NOESY spectrum (Figure S12).

The presence of a single aldehyde functional group was further supported by the reaction of the unknown compound with bisulfite (10 mM), which yielded a product with m/z of 207 (Figure S13). This observation was consistent with previous reports on the detection of aldehyde.[47−49]

The peak area of the aldehyde product, as determined by HPLC-UV analysis at 361 nm, was always proportional to the concentration of phenol produced (Figure 3). This behavior indicated that this compound was not an oxidation product of phenol. Furthermore, the unknown compound was not the

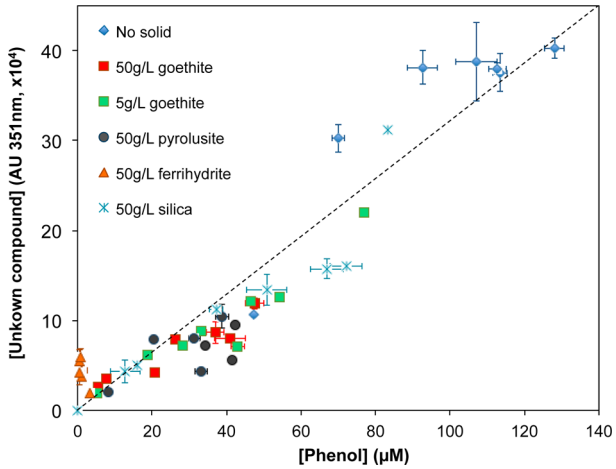

Figure 3. Relationship between phenol concentration and the UV peak intensity of the unknown oxidation product. Samples were collected at different reaction times during benzene oxidation in the presence of persulfate and different concentrations of solids. Initial [benzene] = 1000 μM, initial $[S_2O_8^{2-}]$ = 1000 μM, and pH was buffered at 8.0 with 50 mM borate.

product of direct reaction between phenol and persulfate because the oxidation of phenol by excess persulfate was too slow, and the small loss of phenol that occurred did not result in the formation of the unknown (data not shown). Therefore, it is likely that the aldehyde-like compound was a primary product of the reaction of $SO_4^{\bullet-}$ and benzene. Additional activated persulfate transformation experiments with benzoquinone, hydroquinone, catechol, and 1,2,4-benzenetriol did not produce the same benzene transformation product, indicating that none of these compounds are intermediates in the formation of the ring-cleavage product from the oxidation of benzene.

Previous researchers have described alternative pathways through which aldehyde-like ring cleavage products can be produced directly from $HO^{\bullet}$ attack on benzene.[36,41,50,51] One possibility is the formation of a *meta*-position isomer of $C_6H_7O_3^{\bullet}$ produced from the HCHD radical and its rearrangement to an intramolecular endoperoxide with a dioxygen bond (reaction 20 in Scheme 2), which subsequently decomposes to a carbon-centered aldehyde radical (reaction 21).[41−44,50] The aldehyde radical can react with O_2 and produce an aldehyde-like peroxy radical (reaction 22), followed by the elimination of $HO_2^{\bullet}$ to produce a six-carbon aldehyde product (reaction 23).[41] The proposed aldehyde chemical structure shown in Scheme 2 is one possible product that is consistent with the NMR analysis.

The distribution of products was affected by the dissolved O_2 concentration. Higher concentrations of O_2 favored phenol formation (Figure 4A and Table 1). The N_2-purged solutions (i.e., $[O_2]$ = 3 μM) resulted in the formation of phenol at concentrations that were approximately 30% of those observed under air-saturated conditions (i.e., $[O_2]$ = 250 μM) or 10% of those observed under O_2-supersaturated conditions (i.e., $[O_2]$ = 410 μM). In the absence of O_2, it is possible that HCHD radical was oxidized by $S_2O_8^{2-}$ to generate phenol (reaction 13) and the ring-cleavage product (reaction 14) at different ratios than those observed in the presence of O_2.[34,52] Such a process would serve as a chain propagation reaction, producing one mole of $SO_4^{\bullet-}$ for every mole of $S_2O_8^{2-}$ decomposed (reactions 13−14 in Scheme 2). In the goethite-activated persulfate

DOI: 10.1021/acs.est.5b04815
Environ. Sci. Technol. 2016, 50, 890−898

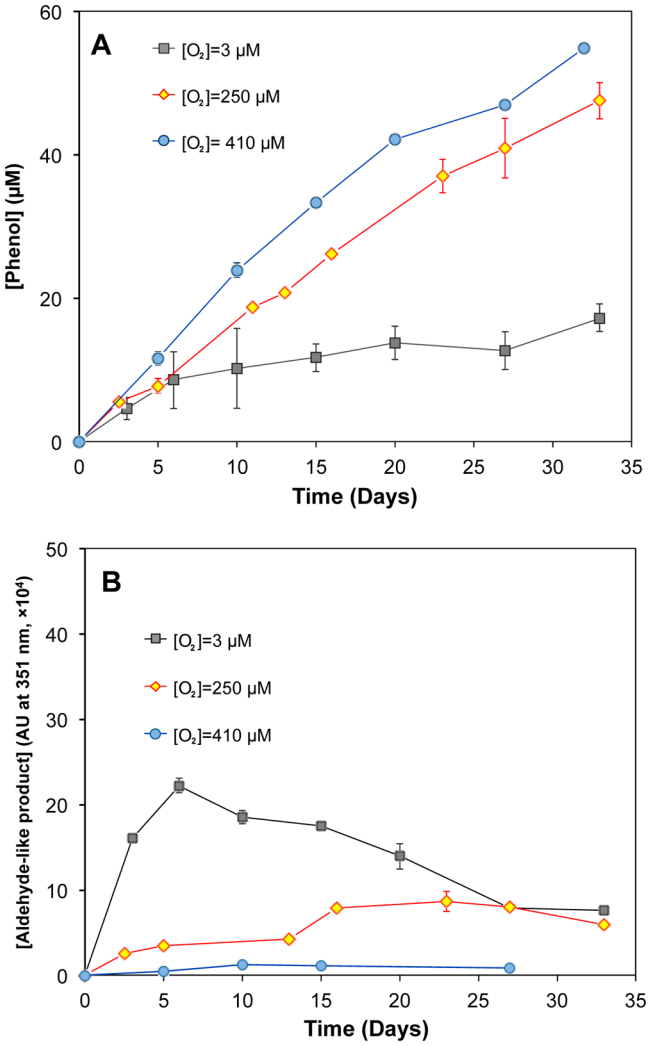

Figure 4. Impacts of dissolved O_2 concentration on oxidation product distribution in the presence of persulfate and solids. (A) Phenol formation; (B) aldehyde-like product. Goethite =50 g/L, initial [benzene] = 1000 μM, initial $[S_2O_8^{2-}]$ = 1000 μM, and pH was buffered at 8.0 with 50 mM borate.

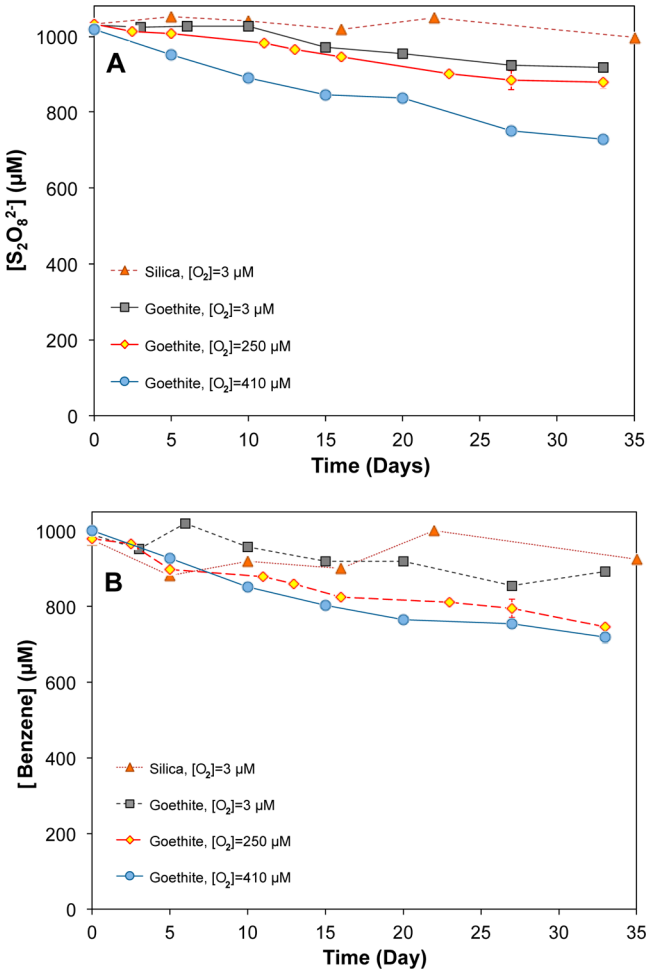

Figure 5. Impacts of dissolved oxygen concentration on the rate of (A) persulfate activation and (B) benzene degradation in the presence of persulfate and solids. Goethite =50 g/L, initial [benzene] = 1000 μM, initial $[S_2O_8^{2-}]$ = 1000 μM, and pH was buffered at 8.0 with 50 mM borate.

system, the concentration of the unknown compound was approximately 10 times higher in the N_2-purged solution ($[O_2]$ = 3 μM) than that in O_2-supersaturated solution ($[O_2]$ = 410 μM) after 5 days of reaction (Figure 4B). A similar trend was observed in ferrihydrite and pyrolusite activated persulfate system (Figure S14). The decrease of the concentration of aldehyde-like product after 10 days of reaction in the N_2-purged solution might due to the acceleration of reaction when dissolved oxygen was accumulated from persulfate activation.

The rate of persulfate activation also decreased at lower dissolved O_2 concentrations when benzene was present (Figure 5A). In the presence of 1 mM benzene and 50 g/L goethite, the amount of persulfate activated decreased from 300 μM to less than 100 μM after 32 days when the initial dissolved O_2 concentration decreased from 410 μM to 3 μM. The same trend was observed for benzene transformation (Figure 5B). These data suggest that as the O_2 concentration decreased, the radical chain reactions slowed down. The results indicated that benzene oxidation and persulfate activation in the absence of oxygen proceeded through different chain reactions (e.g., Reactions 13−14 in Scheme 2). Although it is unlikely that ISCO treatment of groundwater would be completely free of dissolved oxygen, these data strongly suggest that radical chain reactions can be affected by oxygen concentration. The mechanism through which this occurred requires future investigation.

The aldehyde-like compound also was detected when H_2O_2 was activated by minerals and aquifer solids (i.e., the Fenton-like reaction system). Because the amount of benzene that disappeared in the presence of H_2O_2 was much smaller than that observed when $S_2O_8^{2-}$ served as the oxidant (the former was only approximately 10% of the latter), the relative ratio of aldehyde-like compound to phenol concentration was used to compare the product distribution in the two systems. Results indicated that the aldehyde-like compound production decreased dramatically when H_2O_2 was employed as the oxidant compared to when $S_2O_8^{2-}$ was employed as the oxidant (Table S1). For example, in the presence of 50 g/L pyrolusite or ferrihydrite and 1 mM H_2O_2, the aldehyde-like compound was not detected, while a small amount of the product was observed when goethite was used for H_2O_2 activation. The difference in product distribution from benzene oxidation between $S_2O_8^{2-}$ and H_2O_2 activation systems suggests that

DOI: 10.1021/acs.est.5b04815
Environ. Sci. Technol. 2016, 50, 890−898

Table 2. Stoichiometric Efficiency (η) in Metal-Catalyzed System with $S_2O_8^{2-}$ and H_2O_2, Respectively

		$\eta_{H_2O_2}$	$\eta_{S_2O_8^{2-}}$		
		$[O_2]$ = 250 μM	$[O_2]$ = 3 μM	$[O_2]$ = 250 μM	$[O_2]$ = 410 μM
	silica	0.02% ± 0.5%	45% ± 18%	135% ± 71%	–
minerals	goethite	1.02% ± 0.06%	103% ± 18%	145% ± 49%	143% ± 28%
	ferrihydrite	0.01% ± 0.001%	29% ± 11%	26% ± 8%	–
	pyrolousite	0.30% ± 0.02%	28% ± 12%	64% ± 11%	–
clays	nontronite	0.22% ± 0.02%	–	116% ± 17%	–
	montmorillonite	0.12% ± 0.01%	–	138% ± 23%	–
aquifer solids	AWBPH	0.03% ± 0.01%	–	83% ± 25%	–
	AFTCS	0.02% ± 0.01%	–	76% ± 7%	–
	CAROL	0.18% ± 0.04%	–	127% ± 45%	–
	CADOU	0.04% ± 0.01%	–	131% ± 31%	–
	AMTAL	0.02% ± 0.01%	–	106% ± 6%	–

$HO^\bullet$ and $SO_4^{\bullet-}$ propagate different radical chain-reaction pathways.

Oxidant Yield in the Persulfate System. Because benzene is the major sink for $SO_4^{\bullet-}$ under all conditions (reaction 11 in Scheme 2), the disappearance of benzene can be used to identify pathways through which $S_2O_8^{2-}$ decomposes without producing $SO_4^{\bullet-}$. The stoichiometric efficiency is defined as the number of moles of benzene oxidized for every mole of persulfate activated:

$$\eta = \frac{\Delta[\text{benzene}]}{\Delta[S_2O_8^{2-}]} \times 100\% \quad \text{(E1)}$$

Under air-saturated conditions ($[O_2]$ = 250 μM), the stoichiometric efficiency of persulfate activation by different solids ranged from 26% to 145% (Table 2). Most minerals exhibited efficiencies between 83% and 145%. Similar results were observed in synthetic groundwater matrix (Table S2). If $S_2O_8^{\bullet-}$ reacts to produce two additional sulfate radicals (Text S5), the maximum stoichiometric efficiency of the system would be 150%. If $S_2O_8^{\bullet-}$ does not generate additional sulfate radicals, the maximum stoichiometric efficiency could be as low as 50%. Additional research is needed to assess the formation and fate of $S_2O_8^{\bullet-}$ and other species in this system.

There are three possible pathways through which the HCHD radical could be oxidized. First, $S_2O_8^{2-}$ can serve as the oxidant for the HCHD radical (reactions 13−14). Previous studies found $S_2O_8^{2-}$ reacts quickly with a variety of carbon-centered radicals, including aromatic, aliphatic, and semiquinone anion radicals, to generate oxidized products and $SO_4^{\bullet-}$.[2,22,34,52,53] This would lower the stoichiometric efficiency because it only produces one mole of $SO_4^{\bullet-}$ for each mole of $S_2O_8^{2-}$ that decomposes.

Second, the types of mineral surfaces and their surface areas could affect the fate of $SO_4^{\bullet-}$. The oxidant yields for pyrolusite and ferrihydrite were considerably lower (i.e., 26% and 64%, respectively) than other minerals and aquifer solids. Pyrolusite has large structural Mn(IV) content that is known to favor a nonradical pathway for H_2O_2 decomposition.[24] Ferrihydrite has a very large surface area (2 orders of magnitude larger than other minerals)[5] that could favor $SO_4^{\bullet-}$-scavenging reactions:

$$\equiv M^{(n-1)+} + SO_4^{\bullet-} \rightarrow \equiv M^{n+} + SO_4^{2-} \quad \text{(R24)}$$

Third, the HCHD radical is quickly oxidized by O_2 (k = 1.5×10^8 M^{-1} s^{-1}).[36,37] Higher dissolved O_2 concentrations should have decreased the importance of the reaction between HCHD radical and $S_2O_8^{2-}$, resulting in an increase of efficiency. The impact of dissolved O_2 on the stoichiometric efficiency was significant (Table 2). In general, the yield was similar in air- and oxygen-saturation conditions ($[O_2]$ = 250 and 410 μM) but dropped under N_2-purged conditions ($[O_2]$ = 3 μM). For example, the yield dropped by 40% for goethite and pyrolusite when O_2 concentration decreased from 410 μM to 3 μM.

Although the stoichiometric efficiency in the $S_2O_8^{2-}$ system did not reach the theoretical maximum value, it was always 1 to 2 orders of magnitude higher than that observed in the H_2O_2 system (Table 2). This suggest that ISCO systems that employ $S_2O_8^{2-}$ require significantly smaller amounts of oxidant relative to those that use H_2O_2. The inherent inefficiency of H_2O_2-based ISCO is attributed to reactions that result in loss of the peroxide without the production of $HO^\bullet$. Such mechanisms appear to be much less important in the $S_2O_8^{2-}$ system. The inherent disadvantage of the persulfate system, slower activation kinetics than the H_2O_2 system, could be beneficial for remediation because it allows the oxidant to migrate further from the injection point.

The detection of an aldehyde-like product from metal-oxide-catalyzed persulfate and peroxide activation suggests a need for caution in the application of ISCO because aldehyde degradation products such as muconaldehyde have been shown to be responsible for observed benzene toxicity in vivo.[54,55] The potential for generating toxic transformation products during oxidative remediation is already recognized as problematic in drinking water treatment, but it has received less attention in ISCO research. Further studies are needed to understand the formation of the transformation products in ISCO-based remediation systems, to characterize their toxicity, and to assess the potential of these compounds to undergo biotransformation in the subsurface.

■ ASSOCIATED CONTENT

Supporting Information

The Supporting Information is available free of charge on the ACS Publications website at DOI: 10.1021/acs.est.5b04815.

Supplementary text on experimental setup and material preparation, control of dissolved O_2 concentration in samples, high-resolution mass spectrometry and its operating conditions, nuclear magnetic resonance and solid-phase extraction, proposed mechanism on the transformation of $S_2O_8^{\bullet-}$, kinetics of $SO_4^{\bullet-}$ and persulfate radical calculation, kinetics of organic radicals in the benzene/$SO_4^{\bullet-}$ system, and estimate of phenol loss due to direct reaction of $SO_4^{\bullet-}$ or $HO^\bullet$ with phenol

DOI: 10.1021/acs.est.5b04815
Environ. Sci. Technol. 2016, 50, 890−898

in the presence of benzene. Tables showing the characterization of aquifer materials, clay materials, and pure minerals; chemical composition of synthetic groundwater used in this study; comparison of the production of aldehyde-like compound relative to phenol by $S_2O_8^{2-}$ and H_2O_2; and comparison of oxidant yield in synthetic groundwater and MQ water from persulfate activation by different minerals. Figures showing the measurement of total benzene, changes in persulfate concentration and total benzene concentration, identification of aldehyde-like compound as the oxidation product of benzene by $SO_4^{\bullet-}$ radicals, NMR spectra of the unknown compound confirm a ring cleavage product with a fragment identified as an enal, formation of a bisulfite adduct of the unknown ring-cleavage product over time, and formation of aldehyde-like product during persulfate activation by minerals. (PDF)

■ AUTHOR INFORMATION

Corresponding Author

*Phone 510-643-0256; fax 510-642-5319; e-mail: sedlak@berkeley.edu.

Notes

The authors declare no competing financial interest.

■ ACKNOWLEDGMENTS

This research was partially supported by grants to D.L.S. from the U.S. National Institute for Environmental Health Sciences (NIEHS) Superfund Research Program (grant P42 ES004705) at UC Berkeley, to H.L. from the UC Riverside Faculty Initial Complement Research Fund, and to W.L. from the National Science Foundation Graduate Research Fellowship. We thank Dan Borchardt at UC Riverside and Christopher Hill at UC Berkeley for assistance on NMR and Urs Jans at the City College of New York and Manfred Wagner at the Max Planck Institute for Polymer Research in Germany for participation in the project.

■ REFERENCES

(1) Siegrist, R. L.; Crimi, M.; Simpkin, T. J. In situ chemical oxidation: technology, description and status. In *In Situ Chemical Oxidation for Groundwater Remediation*. Springer Media, LLC: New York City, 2011; Chapter 1.

(2) Sra, K. S.; Thomson, N. R.; Barker, J. F. Persistence of persulfate in uncontaminated aquifer materials. *Environ. Sci. Technol.* **2010**, *44*, 3098−3104.

(3) Tsitonaki, A.; Petri, B.; Crimi, M.; Mosbaek, H.; Siegrist, R. L.; Bjerg, P. L. In Situ Chemical Oxidation of Contaminated Soil and Groundwater Using Persulfate: A Review. *Crit. Rev. Environ. Sci. Technol.* **2010**, *40*, 55−91.

(4) Ahmad, M.; Teel, A. L.; Watts, R. J. Persulfate activation by subsurface minerals. *J. Contam. Hydrol.* **2010**, *115*, 34−45.

(5) Liu, H.; Bruton, T. A.; Doyle, F. M.; Sedlak, D. L. In situ chemical oxidation of contaminanted groundwater by persulfate: activation by Fe(III)- and Mn(IV)-containing oxides and aquifer materials. *Environ. Sci. Technol.* **2014**, *48*, 10330−10336.

(6) Antoniou, M. G.; De La Cruz, A. A.; Dionysiou, D. D. Intermediates and reaction pathways from the degradation of microcystin-LR with sulfate radicals. *Environ. Sci. Technol.* **2010**, *44*, 7238−7244.

(7) Anipsitakis, G. P.; Dionysiou, D. D.; Gonzalez, M. A. Cobalt-mediated activation of peroxymonosulfate and sulfate radical attack on phenolic compounds. Implications of chloride ions. *Environ. Sci. Technol.* **2006**, *40*, 1000−1007.

(8) Antoniou, M. G.; De La Cruz, A. A.; Dionysiou, D. D. Degradation of microcystin-LR using sulfate radicals generated through photolysis, thermolysis and e^- transfer mechanisms. *Appl. Catal., B* **2010**, *96*, 290−298.

(9) Guan, Y. H.; Ma, J.; Ren, Y. M.; Liu, Y. L.; Xiao, J. Y.; Lin, L. Q.; Zhang, C. Efficient degradation of atrazine by magnetic porous copper ferrite catalyzed peroxymonosulfate oxidation via the formation of hydroxyl and sulfate radicals. *Water Res.* **2013**, *47*, 5431−5438.

(10) Yang, Y.; Pignatello, J. J.; Ma, J.; Mitch, W. A. Comparison of halide impacts on the efficiency of contaminant degradation by sulfate and hydroxyl radical-based advanced oxidation processes (AOPs). *Environ. Sci. Technol.* **2014**, *48*, 2344−2351.

(11) Drzewicz, P.; Perez-Estrada, L.; Alpatova, A.; Martin, J. W.; Gamal El-Din, M. Impact of peroxydisulfate in the presence of zero valent iron on the oxidation of cyclohexanoic acid and naphthenic acids from oil sands process-affected water intermediates and reaction pathways from the degradation of microcystin-LR with sulfate radicals. *Environ. Sci. Technol.* **2012**, *46*, 8984−8991.

(12) Yuan, S.; Liao, P.; Alshawabkeh, A. N. Electrolytic manipulation of persulfate reactivity by iron electrodes for trichloroethylene degradation in groundwater. *Environ. Sci. Technol.* **2014**, *48*, 656−663.

(13) Huie, R. E.; Neta, P. Chemical behavior of $SO_3^{\bullet-}$ and $SO_5^{\bullet-}$ radicals in aqueous solutions. *J. Phys. Chem.* **1984**, *88*, 5665−5669.

(14) Wardman, P. Reduction potentials of one-electron couples involving free radicals in aqueous solution. *J. Phys. Chem. Ref. Data* **1989**, *18*, 1637−1657.

(15) Neta, P.; Huie, R. E.; Ross, A. B. Rate constants for reactions of inorganic radicals in aqueous solution. *J. Phys. Chem. Ref. Data* **1988**, *17*, 1027−1284.

(16) Buxton, G. V.; Greenstock, C. L.; Helman, W. P.; Ross, A. B.; Tsang, W. Critical review of rate constants for reactions of hydrated electrons, hydrogen atoms and hydroxyl radicals ($^{\bullet}OH/^{\bullet}O^-$) in aqueous solution. *J. Phys. Chem. Ref. Data* **1988**, *17*, 513−886.

(17) Houtz, E. F.; Sedlak, D. L. Oxidative conversion as a means of detecting precursors to perfluoroalkyl acids in urban runoff. *Environ. Sci. Technol.* **2012**, *46*, 9342−9349.

(18) Furman, O. S.; Teel, A. L.; Watts, R. J. Mechanism of base activation of persulfate. *Environ. Sci. Technol.* **2010**, *44*, 6423−6428.

(19) Guan, Y. H.; Ma, J.; Li, X. C.; Fang, J. Y.; Chen, L. W. Influence of pH on the formation of sulfate and hydroxyl radicals in the UV/peroxymonosulfate system. *Environ. Sci. Technol.* **2011**, *45*, 9308−9314.

(20) Lutze, H. V.; Kerlin, N.; Schmidt, T. C. Sulfate radical-based water treatment in presence of chloride: Formation of chlorate, interconversion of sulfate radicals into hydroxyl radicals and influence of bicarbonate. *Water Res.* **2015**, *72*, 349−360.

(21) Zhang, R.; Sun, P.; Boyer, T. H.; Zhao, L.; Huang, C. Degradation of pharmaceuticals and metabolite in synthetic human urine by UV, UV/H_2O_2, and UV/PDS. *Environ. Sci. Technol.* **2015**, *49*, 3056−3066.

(22) Fang, G.; Gao, J.; Dionysiou, D. D.; Liu, C.; Zhou, D. Activation of persulfate by quinones: free radical reactions and implication for the degradation of PCBs. *Environ. Sci. Technol.* **2013**, *47*, 4605−4611.

(23) Petigara, B. R.; Blough, N. V.; Mignerey, A. C. Mechanisms of hydrogen peroxide decomposition in soils. *Environ. Sci. Technol.* **2002**, *36*, 639−645.

(24) Pham, A. L.; Doyle, F. M.; Sedlak, D. L. Kinetics and efficiency of H_2O_2 activation by iron-containing minerals and aquifer materials. *Water Res.* **2012**, *46*, 6454−6462.

(25) Liang, C.; Huang, C. F.; Mohanty, N.; Kurakalva, R. M. A rapid spectrophotometric determination of persulfate anion in ISCO. *Chemosphere* **2008**, *73*, 1540−1543.

(26) Johnson, R. L.; Tratnyek, P. G.; Johnson, R. O. Persulfate persistence under thermal activation conditions. *Environ. Sci. Technol.* **2008**, *42*, 9350−9356.

(27) Yu, X. Y.; Bao, Z. C.; Barker, J. R. Free radical reactions involving $Cl^{\bullet}$, $Cl_2^{\bullet-}$, and $SO_4^{\bullet-}$ in the 248 nm photolysis of aqueous solutions containing $S_2O_8^{2-}$ and Cl^-. *J. Phys. Chem. A* **2004**, *108*, 295−308.

DOI: 10.1021/acs.est.5b04815
Environ. Sci. Technol. 2016, 50, 890−898

(28) Das, T. N. Reactivity and role of $SO_5^{\bullet-}$ radical in aqueous medium chain oxidation of sulfite to sulfate and atmospheric sulfuric acid generation. *J. Phys. Chem. A* **2001**, *105*, 9142−9155.
(29) Kolthoff, I. M.; Miller, I. K. The chemistry of persulfate. I. The kinetics and mechanism of the decomposition of the persulfate ion in aqueous medium. *J. Am. Chem. Soc.* **1951**, *73*, 3055−3059.
(30) Herrmann, H.; Reese, A.; Zellner, R. Time-resolved UV/VIS diode-array absorption spectroscopy of SO_x^- (x = 3, 4, 5) radical anions in aqueous solution. *J. Mol. Struct.* **1995**, *348*, 183−186.
(31) Peyton, G. R. The free-radical chemistry of persulfate-based total organic carbon analyzer. *Mar. Chem.* **1993**, *41*, 91−103.
(32) Zhang, T.; Zhu, H.; Croué, J. P. Production of sulfate radical from peroxymonosulfate induced by a magnetically separable $CuFe_2O_4$ spinel in water: efficiency, stability and mechanism. *Environ. Sci. Technol.* **2013**, *47*, 2784−2791.
(33) Neta, P.; Huie, R. E.; Ross, A. B. Rate constants for reactions of inorganic radicals in aqueous solution. *J. Phys. Chem. Ref. Data* **1988**, *17*, 1027−1284.
(34) Norman, R. O. C.; Storey, P. M.; West, P. R. Electron spin resonance studies. Part XXV. Reactions of the sulphate radical anion with organic compounds. *J. Chem. Soc. B* **1970**, 1087−1095.
(35) Aravindakumar, C. T.; Schuchmann, M. N.; Rao, B. S. M.; Von Sonntag, J.; Von Sonntag, C. The reactions of cytidine and 2′-deoxycytidine with $SO_4^{\bullet-}$ radical revisited. Pulse radiolysis and product studies. *Org. Biomol. Chem.* **2003**, *1*, 401−408.
(36) Pan, X. M.; Schuchmann, M. N.; von Sonntag, C. Oxidation of benzene by the OH radical: a product and pulse radiolysis study in oxygenated aqueous solution. *J. Chem. Soc., Perkin Trans. 2* **1993**, *3*, 289−297.
(37) Von Sonntag, C.; Dowideit, P.; Fang, X.; Mertens, R.; Pan, X.; Nienschuchmann, M.; Schuchmann, H. The fate of peroxyl radicals in aqueous solution. *Water Sci. Technol.* **1997**, *35*, 9−15.
(38) Sedlak, D. L.; Hoigne, J. The role of copper and oxalate in the redox cycling of iron in atmospheric waters. *Atmos. Environ., Part A* **1993**, *27*, 2173−2185.
(39) Kwan, W.; Voelker, B. M. Rates of hydroxyl radical generation and organic compound oxidation in mineral-catalyzed Fenton-like systems. *Environ. Sci. Technol.* **2003**, *37*, 1150−1158.
(40) Keenan, C. K.; Sedlak, D. L. Factors affecting the yield of oxidant from the reaction of nanoparticulate zero-valent iron and oxygen. *Environ. Sci. Technol.* **2008**, *42*, 1262−1267.
(41) Srinivasan, T. K. K.; Balakrishnan, I.; Reddy, M. P. On the nature of the products of γ-radiolysis of aerated aqueous solution of benzene. *J. Phys. Chem.* **1969**, *73*, 2071−2073.
(42) Lemaire, J.; Croze, V.; Maier, J.; Simonnot, M. Is it possible to remediate a BTEX contaminated chalky aquifer by in situ chemical oxidation? *Chemosphere* **2011**, *84*, 1181−1187.
(43) Balakrishnan, I.; Reddy, M. P. The effect of temperature on the γ-radiolysis of aqueous solutions. *J. Phys. Chem.* **1972**, *76*, 1273−1279.
(44) Jacob, N.; Balakrishnan, I.; Reddy, M. P. Characterization of the hydroxyl radical in some photochemical reactions. *J. Phys. Chem.* **1977**, *81*, 17−22.
(45) Levsen, K.; Schiebel, H.; Terlouw, J. K.; Jobst, K. J.; Elend, M.; Preiß, A.; Thiele, H.; Ingendoh, A. Even-electron ions: a systematic study of the neutral species lost in the dissociation of quasi-molecular ions. *J. Mass Spectrom.* **2007**, *42*, 1024−1044.
(46) Bertz, S. H.; Dabbagh, G. Chemistry under physiological conditions. Part 8. NMR spectroscopy of malondialdehyde. *J. Org. Chem.* **1990**, *55*, 5161−5165.
(47) Donnally, L. H. Quantitative determination of formaldehyde and benzaldehyde and their bisulfite addition products. *Ind. Eng. Chem., Anal. Ed.* **1933**, *5*, 91−92.
(48) Ragan, J. A.; am Ende, D. J.; Brenek, S. J.; Eisenbeis, S. A.; Singer, R. A.; Tickner, D. L.; Teixeira, J. J.; Vanderplas, B. C.; Weston, N. Safe execution of a large-scale ozonolysis: Preparation of the bisulfite adduct of 2-hydroxyindan-2-carboxaldehyde and its utility in a reductive amination. *Org. Process Res. Dev.* **2003**, *7*, 155−160.
(49) Kissane, M. G.; Frank, S. A.; Rener, G. A.; Ley, C. P.; Alt, C. A.; Stroud, P. A.; Vaid, R. K.; Boini, S. K.; McKee, L. A.; Vicenzi, J. T.; Stephenson, G. A. Counterion effects in the preparation of aldehyde-bisulfite adducts. *Tetrahedron Lett.* **2013**, *54*, 6587−6591.
(50) Pan, X. M.; Schuchmann, M. N.; von Sonntag, C. Hydroxyl-radical-induced oxidation of cyclohexa-1,4-diene by O_2 in aqueous solution. A pulse radiolysis and product study. *J. Chem. Soc., Perkin Trans. 2* **1993**, *6*, 1021−1028.
(51) Fang, X.; Pan, X.; Rahmann, A.; Schuchmann, H.; von Sonntag, C. Reversibility in the reaction of cyclohexadienyl radicals with oxygen in aqueous solution. *Chem. - Eur. J.* **1995**, *1*, 423−429.
(52) Beylerian, N. M.; Khachatrian, A. G. The mechanism of the oxidation of alcohols and aldehydes with peroxydisulphate ion. *J. Chem. Soc., Perkin Trans. 2* **1984**, *12*, 1937−1941.
(53) Lau, T. K.; Chu, W.; Graham, N. J. D. The aqueous degradation of butylated hydroxyanisole by UV/$S_2O_8^{2-}$: study of reaction mechanisms via dimerization and mineralization. *Environ. Sci. Technol.* **2007**, *41*, 613−619.
(54) Latriano, L.; Goldstein, S. D.; Witz, G. Formation of muconaldehyde, an open-ring metabolite of benzene, in mouse liver microsomes: an additional pathway for toxic metabolites. *Proc. Natl. Acad. Sci. U. S. A.* **1986**, *83*, 8356−8360.
(55) Short, D. M.; Lyon, R.; Watson, D. G.; Barski, O. A.; McGarvie, G.; Ellis, E. A. Metabolism of trans, trans-muconaldehyde, a cytotoxic metabolite of benzene, in mouse liver by alcohol dehydrogenase Adh1 and aldehyde reductase AKR1A4. *Toxicol. Appl. Pharmacol.* **2006**, *210*, 163−170.

DOI: 10.1021/acs.est.5b04815
Environ. Sci. Technol. 2016, 50, 890−898